Proceedings of the ASME 2010 3rd Joint US-European Fluids Engineering Summer Meeting and 8th International Conference on Nanochannels, Microchannels, and Minichannels
FEDSM-ICNMM2010
August 1-5, 2010, Montreal, Canada

FEDSM-ICNMM2010-30184

WATER JET PERFORMANCE VARIATION FOR INTRUSION OF A CYLINDER CENTRAL-BODY

Can Kang
School of Energy and Power Engineering
Jiangsu University
Zhenjiang 212013,China

Shengnan Xiao
School of Energy and Power Engineering
Jiangsu University
Zhenjiang 212013,China

Dong Liu
School of Energy and Power Engineering
Jiangsu University
Zhenjiang 212013,China

Feng Zhang
School of Energy and Power Engineering
Jiangsu University
Zhenjiang 212013,China

ABSTRACT

Based on Karman vortex street principle, central-body nozzle is expected to arouse cavitation in the discharged jet and then result in strong impact on acted object. To discover the influence of central-body on flow characteristics, under the same jet pressure of 15MPa, comparison between the two free water jet fields produced respectively by a central-body nozzle and a round nozzle was conducted. Phase Doppler particle anemometry (PDPA) was applied to measure velocity distribution, turbulent fluctuation and droplet diameter distribution at different traverse sections. Experimental results show that although the annular jet tends to concentrate soon after the central body, the radial diffusion of the jet discharged from the central-body nozzle is more obvious. For the two jets kinetic energy is well remained along the jet direction and high-velocity zone is wider near the jet axis of the central-body nozzle. For the jet discharged from the central-body nozzle, turbulent fluctuation near the jet axis is relatively weak. As for possible cavitation, the position is right after the central body and the reachable distance of cavitation effect is short, which produces an inevitable restriction on the nozzle's application. And similar Sauter mean diameter(SMD) distribution profiles are found in the two jet fields especially when distance between nozzle and traverse section gets large. The study here provides quantitative and comparative information for the two nozzles and can be referred to in further study and optimal design of central-body nozzle.

Key words: central-body nozzle; round nozzle; comparison; cavitation; turbulent fluctuation; droplet distribution

INTRODUCTION

As an effective way of energy transfer, high-pressure water jet technology has been paid a lot of attention since 1970's and its application has been extended to several engineering fields such as cleaning, drilling and cutting [1]. Compared with other processing technologies such as mechanical grinding, laser machining and plasma processing, the most distinct advantage of water jet processing lies in its cold-state operating ability. Continuous high-pressure water jet exerts a transient force on local surface of the acted object. Potential cavitation effect contributes to erosion of acted object's surface as well.

A great number of studies about common round jet flow in both theoretical and experimental views have been reported. Especially in recent years, more advanced computation techniques such as large eddy simulation (LES) have been employed to study those complicated phenomena [2]. Turbulent coherent structures of various scales are also expected to be explained with computational fluid dynamics(CFD) techniques. However, for numerical simulation of high-pressure water jet,

several physical factors such as droplet breakup, droplet evaporation and interaction among droplets need to be comprehensively considered, which is difficult to be handled reasonably with current CFD technology [3].

Several parameters such as magnitude and distribution of kinetic energy, energy dissipation, flow pattern, droplet size and its distribution are generally used to explain the difference between low-pressure and high-pressure water jets. As for high-pressure water jet, rigid requirement is put forward due to large velocity magnitude. There are few reports about quantitative measurement of high-pressure water jet flow field and corresponding flow patterns have not yet been detailedly illustrated. Furhermore, flow field features are helpful for improvement of the whole system's energy-saving ability.

As the energy carrier, droplet in water jet has been consistently stuided although distribution of droplets with various scales is difficult to be captured with general techniques. However, with current flow measurement technology, exact measurement of droplet size distribution can be realized [4]. Crucial turbulent parameters such as root-mean-square (RMS) velocity and Reynolds stress can also be obtained[5]. Even the transit time for a droplet passing through a control volume can be recorded and corresponding probability density function can be built [6].

As a special nozzle, central-body nozzle is proposed for producing cavitation effect after the central body and strengthening the impact on acted object[7]. Here, under the same jet pressure of 12MPa, a round water jet and a jet discharged from a central-body nozzle were studied comparatively. Phase Doppler particle anemometry (PDPA) was used to measure velocity distribution and droplet size distribution. Through flow analysis of six sections along the jet axis, energy features and droplet behavior are expected to be explained and relation between turbulent fluctuation and droplet size distribution is to be illustrated. Further study is performed about the behavior of single droplet at different positions.

NOMENCLATURE

D = diameter of single droplet(μm)
D_{32} = Sauter mean diameter(μm)
D_i = diameter of the size class i (μm)
D_{max} = maximum droplet diameter(μm)
m = number of size classes
N = droplet amount in a sampling group
n_i = number of droplets in ith size class
p = static pressure at nozzle inlet (MPa)
$\bar{u}$ = average velocity in a sampling group (m/s)
u_i = velocity of single droplet (m/s)
u_{rms} = root mean square velocity (m/s)

EXPERIMENTATION

As a non-intrusive measurement method, PDPA has been effectively used in measurement of flow velocity and droplet size. When an object scatters lights, consequent Doppler frequency shift is in relation to travelling speed of the object. Droplet diameter can be obtained from measured phase difference. With PDPA, simultaneous recording of droplet diameter and droplet velocity can be realized. However, three-dimensional synchronous measurement is hard to be accurately achieved according to current level of PDPA[8].

A PDPA system produced by Dantec corporation is applied in this study. The system is composed of an argon ion laser generator with maximum power of 5W, a two-dimensional emission probe, a receiving probe, a fiber driver, a photoelectric receiver, a data processor, control software, a three-dimensional coordinates frame and a displacement framework. For the scattering model of refraction used, a scattering angle of 35° is selected in the experiment. The parameters employed are listed in Table 1.

Table 1. Parameters of the PDPA system

Parameter	Value
Focal length	500 nm
Wavelength	514.5 nm (green laser)
	488.0 nm (blue laser)
Beam spacing	38 mm
Beam diameter	1.35 mm
Fringe spacing	6.775 μm (green laser)
	6.426 μm (blue laser)
Probe volume	0.243 mm×0.243 mm×6.389 mm (green laser)
	0.230 mm×0.230 mm×6.060 mm (blue laser)

A triple-cylinder plunger pump with rated power of 9kW is applied as the pressure-enhancing equipment. The pressure at the pump outlet is 23MPa. Energy losses along the high-pressure tube are taken into account. Through a regulating valve, the jet pressure p is set to be 12MPa. The transmitter probe and receiver probe are fixed on the high-accuracy three-dimensional coordinates frame whose movable components are controlled by a computer. The moving step can be as less as 0.1 mm. Subsequently an ellipsoidal control volume travels in the jet flow with the movement of the coordinates frame. The diameter of the round nozzle is 1.68mm and diameter of the central body is 1.0mm. Characteristic Reynolds number (Re) is 2.6×10^5. Since the medium is tap water, no tracer particles are needed. Schematic view of the experiment system is shown in Fig.1 and two jet flows are displayed in Fig.2.

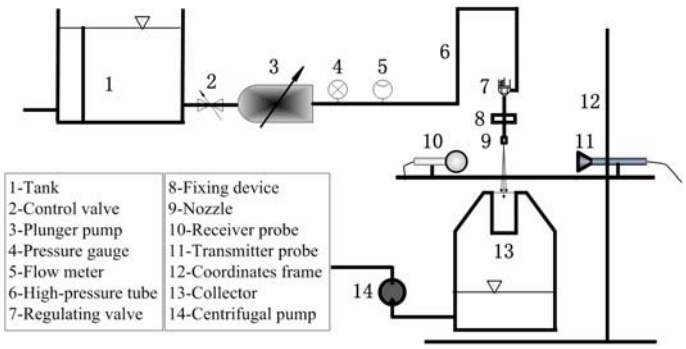

Fig.1 Sketch of the experiment system

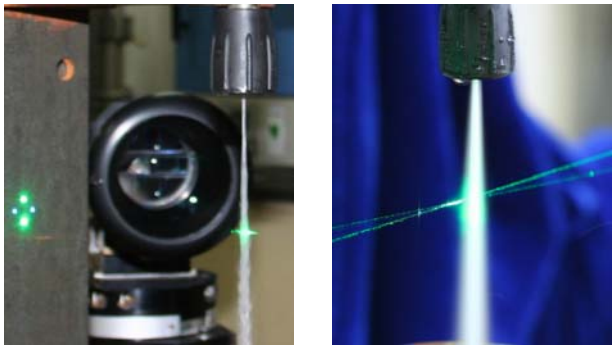

(a) round nozzle (b) central-body nozzle

Fig.2 Two nozzles in situ

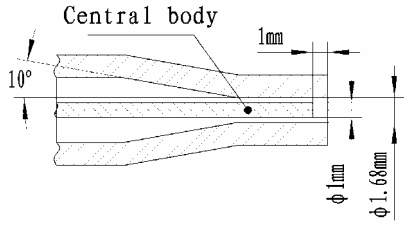

(a) central-body nozzle

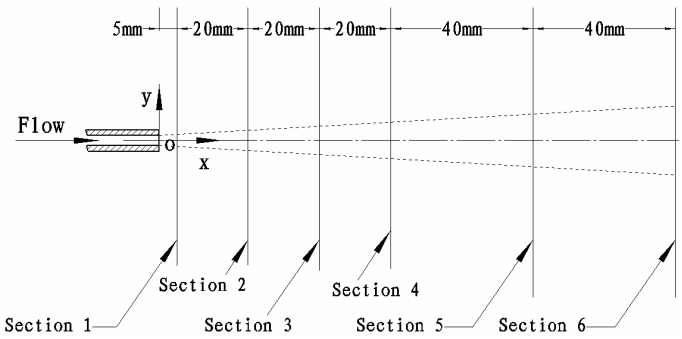

(b) sampling sections

Fig.3 Sketch of central-body nozzle and sampling sections

Fig.3 shows section view of central-body nozzle and positions of six sampling sections. The round nozzle can be obtained through removing the central body from the central-body nozzle with other structures unchanged. Origin of coordinates of a rectangular coordinate system is set at the symmetrical center of nozzle outlet. Y-coordinates is set to be vertical to the jet flow direction. Sampling amount of droplets at each control volume is set to be 2000 in each complete sampling process.

RESULTS AND DISCUSSION

Axial velocity distribution

Axial velocity distribution in the flow field discharged from the central-body nozzle is shown in Fig.4 where the radial position is set by the PDPA control software and the deviation from the centerline is due to vertical inclination of the nozzle-fixing frame. At each section, there is a nearly normal distribution and maximum axial velocity magnitude does not dissipate apparently from Section 1 to Section 6, which proves well maintained kinetic energy along the jet direction. Near the nozzle outlet, traverse distance covered by the jet is relatively short and at Section 6, the jet covers the widest traverse range with smooth distribution occurring near jet rim.

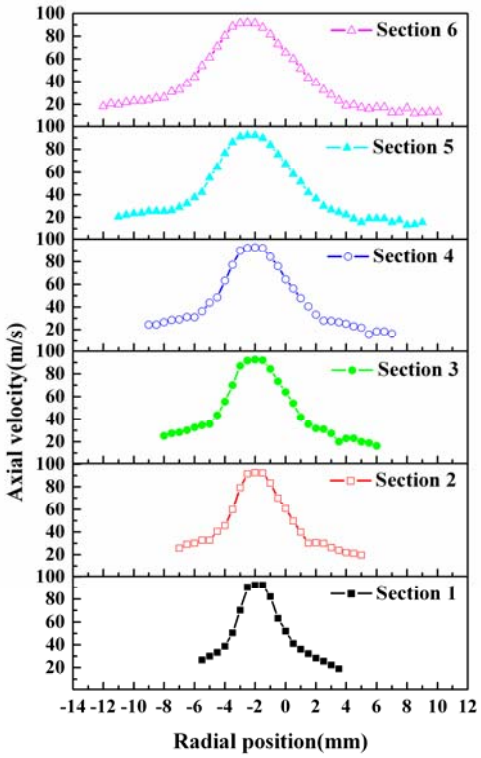

Fig.4 Axial velocity distribution in flow field discharged from central-body nozzle

Axial velocity distribution in flow field discharged from the round nozzle is shown in Fig.5. Being compared with that in

Fig.4, distributions in Fig.5 are more irregular, and peaks in Fig.5 are more protrudent. Peak axial velocities in Fig.5 are uniformly lower than their counterparts in Fig.4 for the change of flow section area due to addition of the central body. Traverse distances covered by the two jets at corresponding section are slightly different. Evident core in round jet is located near the nozzle outlet. The core will gradually disappear with increased distance from the nozzle outlet.

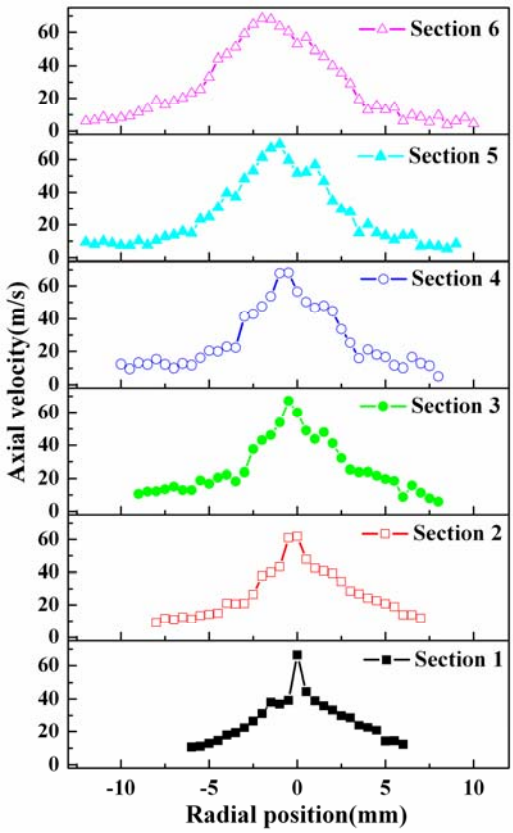

Fig.5 Axial velocity distribution in flow field discharged from round nozzle

Radial velocity distribution

As a generally neglected flow parameter in high-pressure water jet, radial velocity seems to be important in illustration of characteristics of the flow discharged from the annular passage around the central body. Radial velocity distributions of the two flow fields are shown in Fig.6. Better symmetry about the jet axis is found in Fig.6(b) where radial velocity distributions at the six sections in the flow discharged from the central-body nozzle are presented. In Fig.6(a), radial velocity distribution curves at the other five sections mingle with each other near the jet rim except that at Section 1. The magnitude of radial velocity at Section 1 is comparatively high, especially near jet rim. Intense interaction between water jet and ambient air can be predicted just when the jet is discharged from the nozzle. Relatively smooth and discernible distribution in Fig.6(b) indicates that radial velocity tends to be uniform with increased x-distance from the nozzle. Furthermore, the jet profile is easy to be destroyed and subsequently produced small droplets help to improve the efficiency and quality of PDPA sampling.

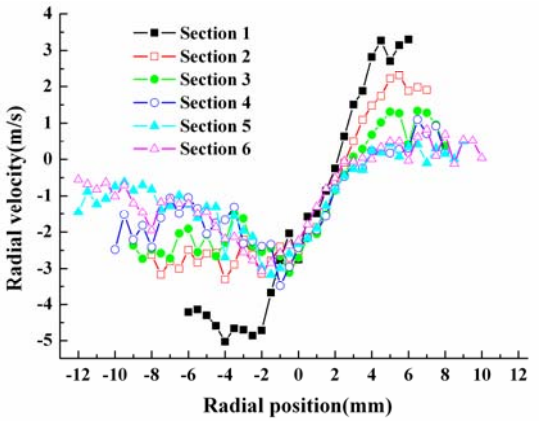

(a) round nozzle

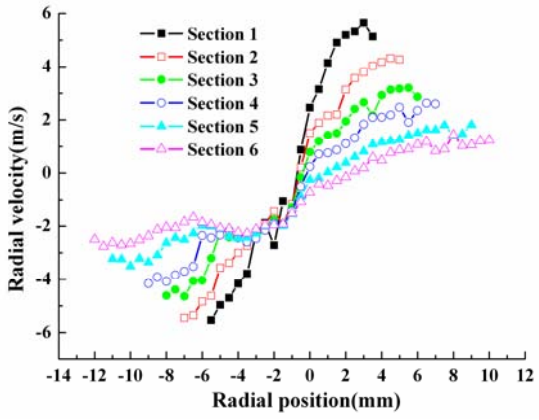

(b) central-body nozzle

Fig.6 Radial velocity distribution

RMS velocity distribution

Root mean square (RMS) velocity is defined by

$$u_{rms} = \sqrt{\frac{1}{N}\sum_{i=0}^{N-1}(u_i - \bar{u})^2} \quad (1)$$

where

$$\bar{u} = \frac{1}{N}\sum_{i=0}^{N-1} u_i \quad (2)$$

Axial RMS velocity distributions in the two flow fields are shown in Fig.7. Remarkable difference is found in Fig.7(a) and Fig.7(b). For the round nozzle in Fig.7(a), distribution curves

representing the six sections mingle with each other. While in Fig.7(b), relatively regular distribution is found and there are two peaks just near the jet center where valley axial RMS velocity appears. It should also be noticed in Fig.7(b) that the large discrepancy between maximum and minimum axial RMS velocity magnitudes is caused by strong interaction near the jet axis.

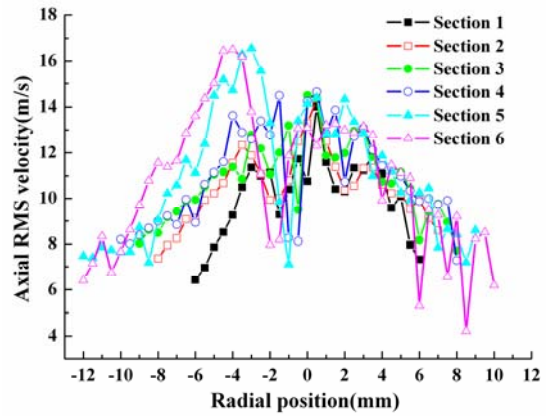

(a) round nozzle

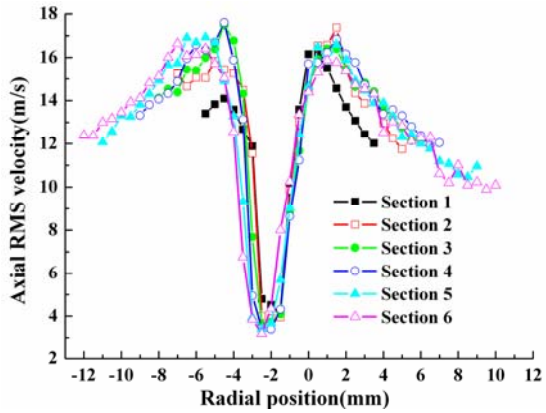

(b) central-body nozzle

Fig.7 Axial root mean square velocity distribution

Radial RMS velocity distributions are shown in Fig.8. Relatively random distribution is found in Fig.8(a) corresponding to the flow field discharged from the round nozzle. Being compared with the radial velocity distribution shown in Fig.6(a), the magnitudes of radial and radial RMS velocity magnitude are equivalent. But in Fig.8(a), obvious difference can be found at the six selected sections. With the distance from the nozzle increased, distribution of radial RMS velocity tends to be uniform along the traverse direction, which can be explained by the continuous development of the jet and mutual interaction between water jet and ambient air. Actually, distribution in Fig.8(b) is similar with that in Fig.8(a). Particularly, near the jet center, valley radial RMS velocity value appears in Fig.8(a) and Fig.8(b). In Fig.8(b), radial RMS velocity keeps increasing towards jet rim, while obvious peak values emerge at jet rim in Fig.8(a).

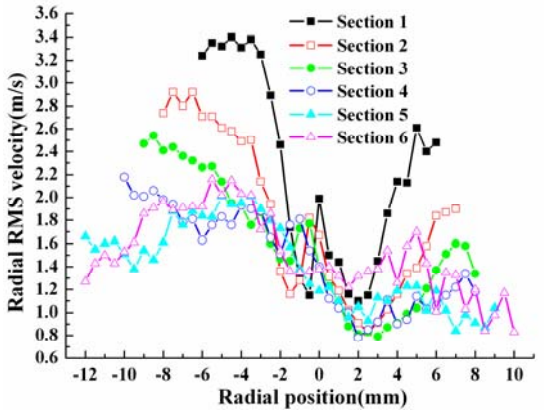

(a) round nozzle

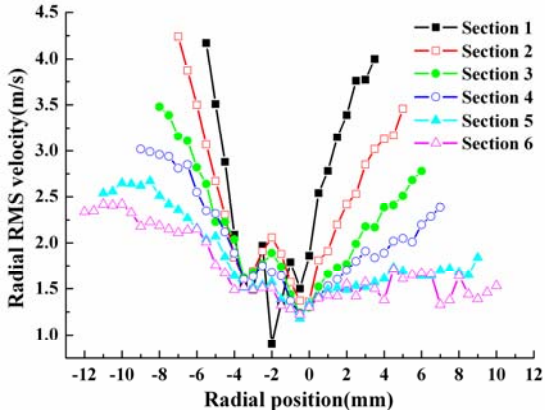

(b) central-body nozzle

Fig.8 Radial root mean square velocity distribution

Distribution of SMD

As an important parameter, Sauter mean diameter is generally used to evaluate the droplet diameter and its distribution in a sampling group. SMD is defined by

$$D_{32} = \frac{\sum_{i=1}^{m} n_i D_i^3}{\sum_{i=1}^{m_i} n_i D_i^2} \tag{3}$$

Fig.9 shows SMD distribution along the jet direction for the two flow fields. For the flow discharged from the round nozzle, discrepancy among the SMD distributions at the six sections is relatively small, although the overall tendencies in Fig.9(a) and Fig.9(b) seem to be similar. Maximum SMD in Fig.9(a) is about 107μm which is less than its counterpart in Fig.9(b).

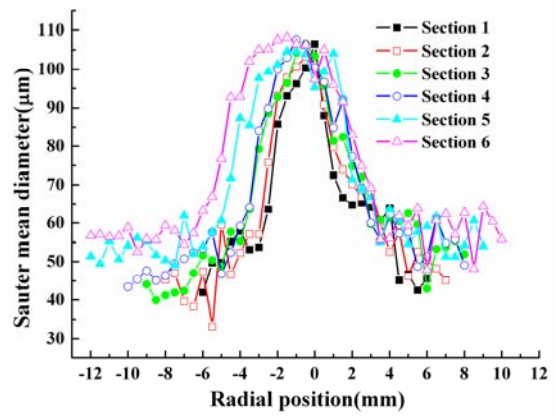

(a) round nozzle

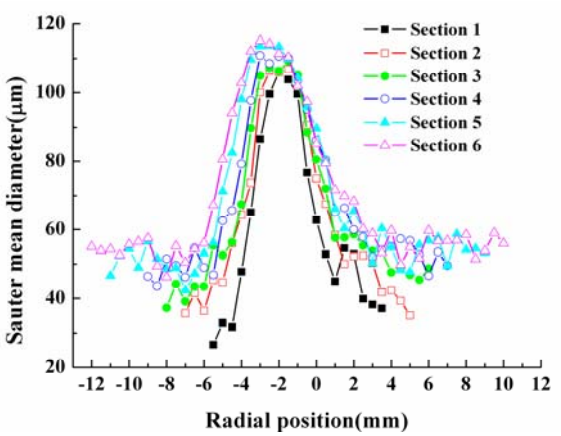

(b) central-body nozzle

Fig.9 Distribution of Sauter mean diameter

The two maximum Sauter mean diameters are uniformly located near the jet axis in Fig.9(a) and Fig.9(b). The break-up mechanism of large droplet in the flow discharged from central-body nozzle is complicated but two factors are inevitably involved, one is the collision among droplets near jet axis, the other is the friction between water jet and ambient air. For the latter, the ability to destroy large droplet's profile is much stronger, which can be discovered from the sharp contrast of SMD distributions at jet center and jet rim in both Fig.9(a) and Fig.9(b).

CONCLUSIONS

There are some obvious differences between flow fields discharged from the round jet nozzle and central-body nozzle, although kinetic energy is well maintained in both the two flow fields. In view of operation, the central-body nozzle is more appropriate for occasions with broad acting area for the relatively diffused jet flow with high kinetic energy near the nozzle outlet.

At different sections along the jet axis, distributions of axial velocity, radial velocity, and even the Sauter mean diameter, show respective similarity for the two flow fields. But for the RMS velocity, particularly the axial RMS velocity, the distribution in flow discharged from the round nozzle is more random. Radial velocity has its peak value near the jet rim, as proves the apparent interaction between water jet and entrained ambient air. Radial velocity contributes much to droplet's breaking up, which is distinctly found in the flow discharging from the central-body nozzle. Although the tendency of SMD distribution is nearly uniform for the two flows, different generation mechanism of small droplet near jet axis and at jet rim can still be discerned through the experiment.

ACKNOWLEDGMENTS

This work is supported by the National Natural Science Foundation of China (Grant No.50806031).

REFERENCES

[1] Xue Suocheng, Zhang Yang, Ma Fei, Gaoyuan, Xue Dexiang. Application of high-pressure water jet flow technique in washing of internal surface of high-pressure pipes. OGST, 2008, 27(9): 45-47.

[2] Fan Quanlin, Zhang Huiqiang, Guo Yincheng, Wang Xilin, Lin Wenyi. Large-eddy simulation of a round turbulent jet under the flow axisymmetric assumption. Journal of Combustion Science and Technology, 2001,7(4):248-251.

[3] Jiang Yong,Liao Guanxuan,Wang Qingan, FanWeicheng. Study on calculating model of droplets collision/coalescence in spray process. Fire Safety Science, 2000, 9(2): 27-30.

[4] M.Iguchi, K.Okita, F.Yamamoto. Mean velocity and turbulence characteristics of water flow in the bubble dispersion region induced by plunging water jet. International Journal of Multiphase Flow, 1998,24(4):523-537.

[5] C. Martínez-Bazán, J.L. Montañés, J.C. Lasheras. Statistical description of the bubble cloud resulting from the injection of air into a turbulent water jet. International Journal of Multiphase Flow, 2002,28: 597-615.

[6] Shen Xiong , Wei Nailong , Peng Tao. Measurement of velocity and size characteristics of water spray droplets with a laser phase doppler system. Experiments and Measurements in Fluid Mechanics. 2000, 14(2): 54-60.

[7] David A.Summers. Consideration in the comparison of cavitating and plain water jets. Proceedings of the 2nd U.S. Water Jet Conference, May 24-26, 1983, pp.178-183.

[8] Xia Zhenyan, J iang Nan. The measurement on the turbulence jet with 3D LDV system. Experiments and Measurements in Fluid Mechanics, 2002,16(2):72-77.